ACS APPLIED MATERIALS & INTERFACES

www.acsami.org Research Article

Charge-Carrier Dynamics at the $CuWO_4$/Electrocatalyst Interface for Photoelectrochemical Water Oxidation

Parisa Shadabipour, Austin L. Raithel, and Thomas W. Hamann*

Cite This: *ACS Appl. Mater. Interfaces* 2020, 12, 50592–50599 Read Online

ACCESS | Metrics & More | Article Recommendations | Supporting Information

ABSTRACT: Unraveling the charge-carrier dynamics at electrocatalyst/electrode interfaces is critical for the development of efficient photoelectrochemical (PEC) water oxidation. Unlike the majority of photoanodes investigated for PEC water oxidation, the integration of electrocatalysts with $CuWO_4$ electrodes generally results in comparable or worse performance compared to the bare electrode. This is despite the fact that the surface state recombination limits the water oxidation efficiency with $CuWO_4$ electrodes, and an electrocatalyst ought to bypass this reaction and improve performance. Here, we present results that deepen the understanding of the energetics and electron-transfer processes at the $CuWO_4$/electrocatalyst interface, which controls the performance of such systems. $Ni_{0.75}Fe_{0.25}O_y$ (denoted as Ni75) was chosen as a model electrocatalyst, and through dual-working electrode experiments, we have been able to provide significant insight into the role of the electrocatalyst on the charge-transfer process at the $CuWO_4$/Ni75 interface. We have shown a lack of performance improvement for $CuWO_4$/Ni75 relative to the bare electrode to water oxidation. We attribute this surprising result to water oxidation on the $CuWO_4$ surface kinetically outcompeting hole transfer to the Ni75 electrocatalyst interface.

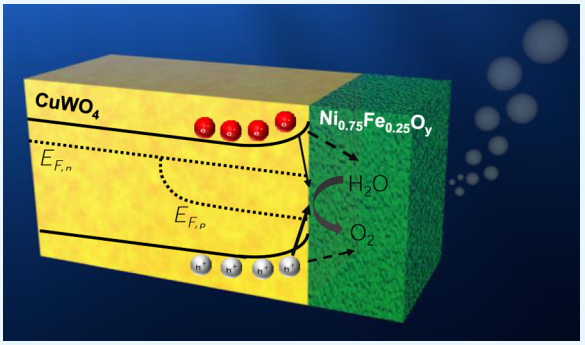

KEYWORDS: *water splitting, photoelectrochemical, $CuWO_4$, nickel–iron oxide, shunting, dual-working electrode (photo)electrochemistry*

INTRODUCTION

Water oxidation is generally the bottleneck half-reaction for solar-to-fuel energy conversion, including water splitting. Metal oxides are an attractive class of materials for photoelectrochemical (PEC) water oxidation due to their high stability and sufficiently positive valence band positions. Binary oxides such as TiO_2, hematite (α-Fe_2O_3), and WO_3 have long been studied as photoanodes for the water oxidation reaction.[1−8] In contrast, the use of ternary and quaternary oxides has emerged as an attractive alternative for PEC applications, in large part owing to their diversity and flexibility in tuning their properties.[9,10] One example is $CuWO_4$ as a photoanode material, which is comprised of earth-abundant elements and has a relatively small band gap of 2.3 eV,[11] making it suitable for light harvesting in the visible region. $CuWO_4$ also remains highly stable in neutral and slightly basic conditions during PEC water oxidation.[12−14] However, $CuWO_4$ exhibits relatively low water oxidation efficiency with the best-reported photocurrent density of only 0.5 mA cm^{-2} at water oxidation standard potential (1.23 V vs RHE), and a photocurrent onset potential that is several hundred millivolts positive with respect to the material's flat band potential.[12,15−17] The low efficiency can be attributed to a combination of inefficient charge separation and hole collection.[12,17,18] Strategies such as nanostructuring[19] and doping[20] can improve charge separation efficiency. By contrast, the poor hole collection efficiency, which originates from a slow reaction kinetics on the $CuWO_4$ surface compared to the competing rate of carrier recombination at mid-gap surface states,[21,22] is expected to improve upon integrating an electrocatalyst overlayer. However, unlike nearly all other photoanodes, the use of electrocatalysts on $CuWO_4$ has not shown promise for improving the efficiency of PEC water oxidation.

Improving the hole collection efficiency through developing an efficient electrocatalyst requires a fundamental understanding of carrier generation and transfer reactions at the interface, which remains a significant research challenge. The enhancement of PEC water oxidation upon the integration of electrocatalyst has been attributed to a variety of causes, including a decrease of surface state recombination,[23,24] increased band bending,[25,26] and improving charge separation.[27,28] Despite the disagreement of specific causes, there is a

Received: August 14, 2020
Accepted: October 16, 2020
Published: October 29, 2020

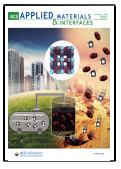

https://dx.doi.org/10.1021/acsami.0c14705
ACS Appl. Mater. Interfaces 2020, 12, 50592–50599

broad agreement of consistent observations that electrocatalysts improve the performance of metal oxide photoanodes. Beyond that, using advanced dual-working electrode (DWE) photoelectrochemistry, Boettcher and co-workers unambiguously demonstrated that the electrocatalyst overlayers serve as a water oxidation catalyst as well as a hole storage layer for hematite photoanodes.[29] Interestingly, the $CuWO_4$/electrocatalyst junction is an unusual exception. We and others have found that catalysts often do not influence the photocurrent onset potential and, in some cases, decrease the activity toward water oxidation reaction. We note, however, that there are a few reports that suggest moderate improvement of $CuWO_4$ photoanodes after electrocatalyst deposition for PEC water oxidation[15,21,30,31]

In this work, we provide new insight into the charge-carrier dynamics at the $CuWO_4$/electrocatalyst interface using DWE photoelectrochemistry. $Ni_{0.75}Fe_{0.25}O_y$ (Ni75) was chosen as a model electrocatalyst to probe the interface due to the high electrocatalytic activity for the water oxidation reaction.[32,33] $CuWO_4$ and Ni75 films were prepared via atomic layer deposition (ALD) and photochemical metal-organic deposition (PMOD), respectively.[11,34] Prior to catalyst deposition, $CuWO_4$ photoanodes were modified with poly(phenylene oxide) (PPO) to eliminate shunting.[35] By directly measuring the potential and the current flowing through the electrocatalyst layer, we reveal that the lack of efficiency improvement for water oxidation is due to inefficient transfer of the photogenerated holes to the electrocatalyst overlayer. Our results provide new insights regarding the dynamic of $CuWO_4$/Ni75 interface during the water oxidation reaction, incentivizing further development and mechanistic investigations of this system, which can be leveraged to improve the performance.

EXPERIMENTAL SECTION

Atomic Layer Deposition of $CuWO_4$. $CuWO_4$ thin films were prepared on fluorine-doped tin oxide (FTO)-coated glass substrates (Hartford Glass, TEC 15, 12 Ω cm^{-2}) via atomic layer deposition using our previously developed procedure.[21] FTO substrates were cleaned by sequential sonication in soap, water, and isopropyl alcohol for approximately 15 min each, followed by drying under a stream of nitrogen. The precursors for deposition of WO_3 and CuO were bis(*tert*-butylimido)bis(dimethylamido)tungsten (VI) ($(tBuN)_2(Me_2N)_2W$) (Strem Chemicals Inc., >97%) and copper(I)-*N*,*N*′-di-sec-butylacetamidinate ($[Cu(sBu\text{-}amd)]_2$) (Dow Chemical Co., >99.0%). We have synthesized the copper precursor at a similar purity, which was also used. Two thousand ALD cycles of WO_3 were first deposited on FTO substrates.[36] During the deposition, the ($(tBuN)_2(Me_2N)_2W$) cylinder was heated to 75 °C and the vapor pulsed for 2 s, followed by 10 s of exposure mode and a 6 s nitrogen purge. A 0.5 s pulse of deionized water (millipore, 18 MΩ cm) was then introduced as the oxidant followed by 15 s of exposure mode and 6 s of purge time to oxidize the tungsten precursor to form amorphous WO_3. Then, 340 cycles of CuO were deposited on the WO_3 films, calculated to result in a 1:1 ratio between two metals according to previous work.[11] The ($[Cu(sBu\text{-}amd)]_2$) cylinder was heated to 150 °C and the vapor pulsed for 3 s in each ALD cycle. The oxidation was performed after purging for 6 s. Then, 10 cycles of ozone (~10% by weight O_3 in ultrahigh purity O_2 produced by Yanco Industries ozone generator) was used as the oxidant and pulsed for 2 s, followed by a 3 s purge. After the deposition of CuO on WO_3, the binary oxides were annealed at 550 °C in air for 30 min with a ramping rate of 2 °C min^{-1}. The $CuWO_4$ thickness was calculated to be 200 nm using spectroscopic ellipsometry and measuring the thickness of the film grown on a spectator silicon wafer substrate (Horiba Jobin Yvon, Smart-SE).

Synthesis of ($[Cu(sBu\text{-}amd)]_2$). Sec-butylamine (99%) and $La(OTf)_3$ were purchased from Oakwood Chemical, and sec-butylamine was dried over activated 3 A molecular sieves for 3 days and $La(OTf)_3$ was activated by heating to 190 °C for 3 days under vacuum. Diethyl ether was purchased from Fisher Scientific and was prepared by drying over activated 3 A molecular sieves for 3 days, degassing, and storing in a nitrogen-filled glovebox for use. CuCl (≥99.995%) and MeLi (1.6 M in diethyl ether) were purchased from Sigma-Aldrich and were used as received. Deuterated benzene-d_6 was purchased from Cambridge Isotopes and used as received. *N*,*N*′-di-sec-butylacetamidine was prepared as reported previously.[37] ($[Cu(sBu\text{-}amd)]_2$) was prepared by modifying a previously reported procedure as described below.[38]

Typically, 8.40 g (49 mmol) of *N*,*N*′-di-sec-butylacetamidine was dissolved in 100 mL of dry diethyl ether in a 200 mL round-bottom flask under nitrogen. The flask was cooled to −30 °C and then allowed to stir at −30 °C for 30 min. Then, 3.85 mL of MeLi (1.6 M in diethyl) was added dropwise to the solution. The flask was allowed to warm to room temperature and was then stirred for 2 h. The solution was then canula transferred to another 200 mL round-bottom containing 4.88 g of CuCl (49 mmol) and 30 mL of dry diethyl ether. The solution was allowed to stir for 18 h and was then filtered under nitrogen and then dried by vacuum. The resulting brown solid was then collected inside a nitrogen-filled glovebox and was then sublimated onto a cold finger under vacuum at 95 °C. A white crystalline powder was collected from the cold finger (4.8024 g, 41.6%). ^{1}H nuclear magnetic resonance (NMR) (500 MHz, benzene-d_6) δ 3.13 (m, 2H), 1.73−1.57 (m, 5H), 1.50 (m, 2H), 1.17 (dt, J = 6.3, 1.6 Hz, 6H), and 0.95−0.86 (m, 6H).

Catalyst Deposition. $Ni_{0.75}Fe_{0.25}O_y$ (Ni75) electrocatalysts were deposited on 1 cm^2 of freshly prepared, and PPO-modified $CuWO_4$ photoanodes by spin coating the metal precursor solution.[34,39] Before catalyst deposition, $CuWO_4$ films were rinsed with deionized water and dried under nitrogen. An appropriate amount of metal precursors, iron (III) 2-ethyl hexanoate (50% w/w in mineral spirits, Strem Chemicals) and nickel (II) 2-ethyl hexanoate (78% w/w in 2-ethyl hexanoic acid, Strem Chemicals), were dissolved in hexane to give a total concentration of 15% w/w metal complex. Approximately, 250 μL of the precursor solution was placed on the substrate, followed by spinning at 3000 rpm for 60 s. The as-prepared $CuWO_4$/Ni75 was treated with UV light to decompose organic residue (254 nm, 4 W) for 2 h followed by annealing in a preheated furnace at 100 °C in air for 1 h. The thickness of the Ni75 film was measured to be ~220 nm using atomic force microscopy (AFM) and spectroscopic ellipsometry.

Electrodeposition of Poly(phenylene oxide) (PPO). PPO blocking layers were selectively polymerized onto any exposed FTO of $CuWO_4$ electrodes. The PPO electrodeposition was performed according to the previous report.[40] Briefly, $CuWO_4$ electrodes were placed in a solution consisting of 90 mM 2-allylphenol, 60 mM phenol, and 100 mM $LiClO_4$ in 10/10/1 water/ethanol/2-butoxyethanol. Ten millimolar tetrabutylammonium hydroxide in methanol was added to the solution to adjust the pH at 9.0. Then, electrodeposition of PPO was done by scanning the electrode potential in the dark with the scan rate of 100 mV s^{-1} from 0.1 to 1.5 V vs Ag/AgCl for 60−80 cycles. To remove unreacted monomers and oligomers, we then soaked electrodes in 10 mM tetrabutylammonium hydroxide in methanol, rinsed with ethanol, and cured in the air at 150 °C for 30 min. Ellipsometry (Horiba Jobin Yvon, Smart-SE) was used to measure the thickness of the PPO layer on a silicon wafer coated with gold and subjected to the same polymerization treatment as described above, which was ~12 nm.

Fabrication of Dual-Working Electrode Devices. To prepare $CuWO_4$ + PPO|$Ni_{0.75}Fe_{0.25}O_y$|Au devices, electrical contact was made to the FTO|$CuWO_4$ + PPO substrate coated with the Ni75 film using silver paste and copper wire to make the first working electrode (WE1). These electrical connections were covered with insulating epoxy (Loctite Hysol 1C) to keep them isolated from the electrolyte during measurements. A 12 nm thick layer of Au was evaporated from the Au metal in an aluminum boat using a vacuum thermal evaporator

https://dx.doi.org/10.1021/acsami.0c14705
ACS Appl. Mater. Interfaces 2020, 12, 50592−50599

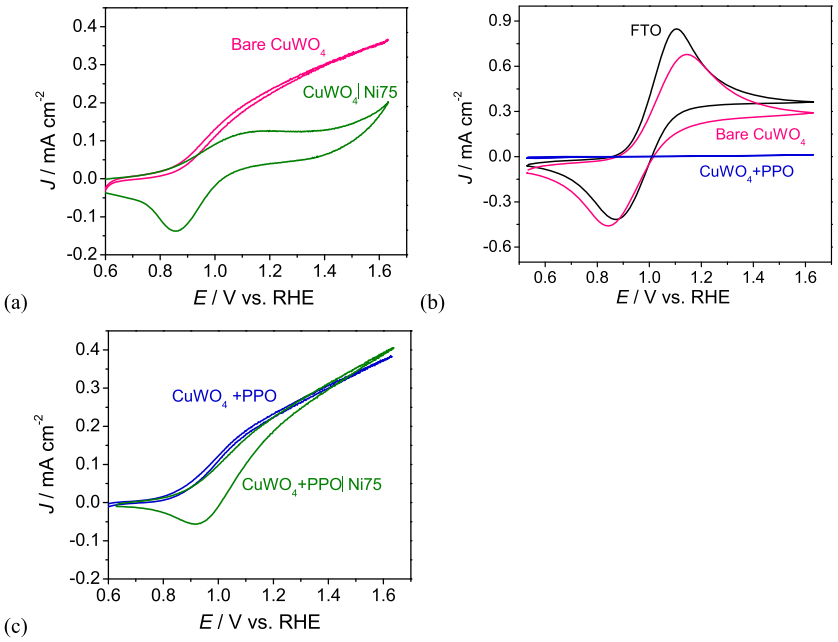

Figure 1. Effect of shunting pathways on $CuWO_4$ performance for water oxidation. (a) J–E responses of the bare $CuWO_4$ (pink), and after deposition of Ni75 (green) under illumination. (b) Dark CV responses of the bare FTO (black), bare $CuWO_4$ (pink), and PPO-modified $CuWO_4$ (blue) in 1.0 M KB_i containing 10 mM $k_4[Fe(CN)_6]$ solution. (c) J–E responses of $CuWO_4$ after modification with PPO (blue) and after deposition of Ni75 (green) under illumination. All measurements were done in 1.0 M KB_i, the scan rate of 20 mV s^{-1}.

(rate = 2 Å s^{-1}) onto the catalyst surface and epoxy around the electrode. The second electrical contact was made to the Au using silver paste and copper wire to produce the second working electrode (WE2) and also covered with insulating epoxy. The first wire was placed inside a glass tube. The second wire was coiled around the glass tube, and then it was inserted into the second glass tube and sealed with hot glue. The voltages and current densities of FTO|$CuWO_4$ + PPO and the Ni75 film were controlled and measured via WE1 and WE2, respectively. The gathered E_{WE2} and J_{WE2} hence give *a* measure of the potential of the electrocatalyst layer (E_{cat}) and current density flowing through the electrocatalyst layer (J_{cat}), respectively. Scheme S1 shows the structure and the digital image of $CuWO_4$ + PPO|$Ni_{0.75}Fe_{0.25}O_y$|Au device.

(Photo)electrochemical Measurements. All electrochemical and photoelectrochemical measurements were performed in a custom-made electrochemical cell setup with an Eco Chemie Autolab potentiostat (Nova electrochemical software). Photoelectrochemical measurements were done in the back-illumination configuration (photons passing through the glass substrate before reaching the semiconductor electrode). A high surface area Pt mesh and homemade saturated Ag/AgCl were used as a counter and reference electrode, respectively. All (photo)electrochemical measurements were carried out at room temperature and in 1.0 M potassium borate (KB_i) buffered at pH 9.0 using KOH pellets and 1.0 M H_3BO_3 (Fisher Scientific Accumet pH meter). Aqueous solutions were prepared with ultrapure water (resistivity 18 MΩ cm) from a Milli-Q water purifier.

A 450 W Xe arc lamp (Horiba Jobin Yvon) was used as a white light source with an AM 1.5 solar filter to obtain a simulated solar spectrum with 100 mW cm^{-2} (1 sun) intensity. Pure photocurrent densities (J_{photo}) were obtained by subtracting the current density in the dark (J_{dark}) from the total current density under illumination (J_{total}). All electrochemical potentials were converted to the reversible hydrogen electrode (RHE) by the equation $E_{RHE} = E_{Ag/AgCl} + 0.197 + pH\ (0.059)$.

Material Characterization. The scanning electron microscope (SEM) images were obtained using SEM (Carl Zeiss Auriga, Dual Column FIBSEM). Raman spectra were collected via Raman microprobe (Renishaw) equipped with a 45 W cobalt DPSS laser (532 nm line) laser and a 100× magnification objective to focus the laser on the film surface. The roughness of the surface was examined by AFM using MFP-3D from Asylum Research.

RESULTS AND DISCUSSION

Two hundred nanometers thin films of $CuWO_4$ were prepared via ALD on fluorine-doped tin oxide (FTO) substrates following the procedure reported previously.[11] The hole collection efficiency (η_{HC}) of $CuWO_4$ for water oxidation was determined by comparing the photocurrent density as a function of the applied potential (J–E) responses of a $CuWO_4$ photoanode for both water oxidation and Na_2SO_3 oxidation (Figure S1). Na_2SO_3 has previously been shown to be a suitable hole scavenger for $CuWO_4$, resulting in quantitative hole collection efficiencies.[12] Similar to this previous report, we observed a cathodic shift of the photocurrent onset potential for hole scavenger oxidation compared to water oxidation.[12] This implies that the η_{HC} at the surface of $CuWO_4$ is limited by surface state recombination. The integration of an electrocatalyst ought to improve the η_{HC} of the photoelectrode for the water oxidation reaction, which would be reflected in an improved photocurrent onset potential.[27,41−43]

The Ni-rich phases of $Ni_xFe_{1-x}O_y$ are known for their fast electrocatalytic activity and electrical conductivity compared to the Fe-rich phases of the electrocatalyst.[32] Thus, we choose $Ni_{0.75}Fe_{0.25}O_y$ (Ni75) to investigate the effect of electrocatalysts on the performance of $CuWO_4$ photoanodes for PEC water oxidation by measuring the J–E responses of the bare electrode and with the addition of the Ni75 electrocatalyst. A smooth ∼220 nm thick Ni75 electrocatalyst was deposited at the surface of the $CuWO_4$ photoanode via the PMOD method from its precursor solution (see Figure S2 and the explanation in the Experimental Section for the characterization of the catalyst thickness). In this method, the annealing time after catalyst deposition is vital to decompose all organic precursors. We used Raman spectroscopy to track the ligand residue at the surface, and we found a 2 h UV illumination was sufficient to

https://dx.doi.org/10.1021/acsami.0c14705
ACS Appl. Mater. Interfaces 2020, 12, 50592−50599

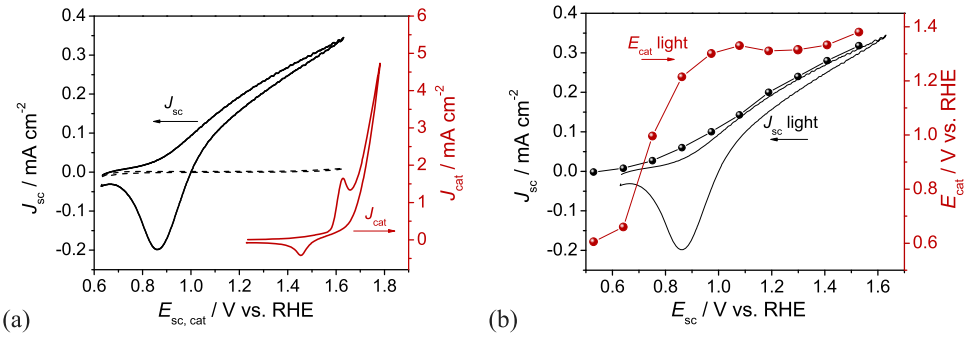

Figure 2. DWE PEC characterization of the electrocatalyst. (a) J–E curve of $CuWO_4$ (sc) and Ni75 (cat) that are collected separately through WE1 and WE2, respectively. (b) Superimposition of E_{cat}, steady-state current density, and J–E curve of $CuWO_4$ that are measured under illumination.

decompose all organic residues (Figure S3). Figure 1a shows the J–E responses under illumination of a $CuWO_4$ photoanode in contact with 1.0 M potassium borate (KB_i) aqueous electrolyte at pH 9.0 before (pink line) and after Ni75 deposition (green line). The deposition of Ni75 on $CuWO_4$ leads to a dramatic decay of the electrode performance for PEC water oxidation with the formation of a capacitive peak at 0.85 V vs RHE corresponding to the Ni^{3+} reduction on the $CuWO_4$ surface. The decreased PEC performance following the Ni75 integration can be caused by shunting effect from direct contact between the electrocatalyst and the conductive FTO substrate.[33]

To determine if the $CuWO_4$ electrodes are susceptible to shunting, the dark cyclic voltammogram (CV) response of the electrode was compared to that of bare FTO electrodes in a 10 mM ferri/ferrocyanide solution (Figure 1b). The reversible redox wave appears on the $CuWO_4$ (pink line) is similar to the wave for bare FTO (black line), albeit with a smaller peak height and higher peak separation, which corresponds to the charge transfer between the ferri/ferrocyanide and the exposed FTO. A similar observation was previously reported for the porous hematite and $BiVO_4$ photoelectrodes.[33,35,44] Recently, we reported a general method to overcome such shunting recombination via selective electrodeposition of a thin PPO insulating layer onto the exposed transparent conductive oxide substrate before electrocatalyst deposition.[35] We, therefore, subjected the $CuWO_4$ electrode to PPO electrodeposition through a series of CV measurements in a phenol and allylphenol solution (Figure S4a). The absence of the redox wave in a ferrocyanide solution after the PPO electrodeposition confirms the blocking of all exposed FTO (Figure 1b, blue line). The lack of exposed FTO on the PPO-modified $CuWO_4$ can also be confirmed by comparing the J–E responses of the bare $CuWO_4$ against $CuWO_4$ modified with PPO in 0.5 M $NaSO_3$ (Figure S4b). Bare $CuWO_4$ has a significant dark current when it is in contact with Na_2SO_3, which is due to the exposed FTO; this dark current is absent after modification of the electrode with PPO. Also, it is important to note that the PEC performance of the $CuWO_4$ photoanode for water oxidation remains the same after PPO modification, suggesting that PPO does not compromise the performance of the $CuWO_4$ (Figure S4c).

Figure 1c shows the J–E behavior of PPO-modified $CuWO_4$ electrodes, with and without the integration of a Ni75 electrocatalyst, in contact with 1.0 M KB_i aqueous electrolyte. As shown, the presence of PPO eliminated diminished performance due to the shunting effects. However, the electrocatalyst does not improve the $CuWO_4$ performance for PEC water oxidation. Also, we have shown that the deposition of a thin film of Ni75 on $CuWO_4$ does not cause a significant shunting but still does not improve the photocurrent onset potential of $CuWO_4$ electrodes without the protective PPO layer for PEC water oxidation (Figure S5). These results are in contrast to what is generally observed for hematite and other metal oxide semiconductors, where cocatalysts improve the PEC water oxidation performance; however, it is in general agreement with literature on $CuWO_4$.[21,45−50] We, therefore, attribute the lack of improvement to a unique aspect of $CuWO_4$ in controlling the electron dynamics at the semiconductor/electrocatalyst interface.

To gain an understanding of the charge-carrier dynamics at the interface of $CuWO_4$/Ni75 and to characterize the electrocatalyst, we fabricated dual-working electrode (DWE) devices pioneered by Boettcher et al.[51] In the DWE technique, the semiconductor photoanode serves as the first working electrode (WE1), and a thin electrolyte-permeable gold (Au) layer at the surface of the electrocatalyst serves as the second working electrode (WE2). Such a configuration allows independent monitoring of the electrocatalyst potential or the current flowing through the electrocatalyst via WE2 while controlling the potential or monitoring the current of the semiconductor photoanode via WE1. Deposition of a pin-hole-free electrocatalyst on the semiconductor surface is essential in the DWE technique to avoid any shorts between gold and the semiconductor or the underlying conductive substrate. Therefore, a smooth and crack-free Ni75 electrocatalyst was deposited via PMOD on a PPO-modified $CuWO_4$ photoanode. The deposition of Ni75 electrocatalyst on $CuWO_4$ reduced the root-mean-squared surface roughness from 20 to 2 nm (Figure S6). This smoothness is essential for having an interconnected gold film on the electrocatalyst surface. A thin, electrolyte-permeable, gold (Au) film was then applied to the electrocatalyst surface to make the $CuWO_4$|Ni75|Au DWE device.

The Ni75 film was conditioned by measuring a series of CVs from WE2 in the dark and from WE1 under illumination to make the electrocatalyst ion permeable. Figure 2a shows the J–E curves collected separately from WE1 and WE2 of $CuWO_4$ (black line) and Ni75 (red line), respectively, after conditioning the electrocatalyst. The J–E response of the electrocatalyst after conditioning is similar to the Ni75 J–E response on the FTO substrate with the Ni^{2+} oxidation peak at 1.65 V vs RHE and the Ni^{3+} reduction peak at 1.45 V vs RHE (Figure S7). The J–E response of $CuWO_4$ measured via WE1

https://dx.doi.org/10.1021/acsami.0c14705
ACS Appl. Mater. Interfaces 2020, 12, 50592−50599

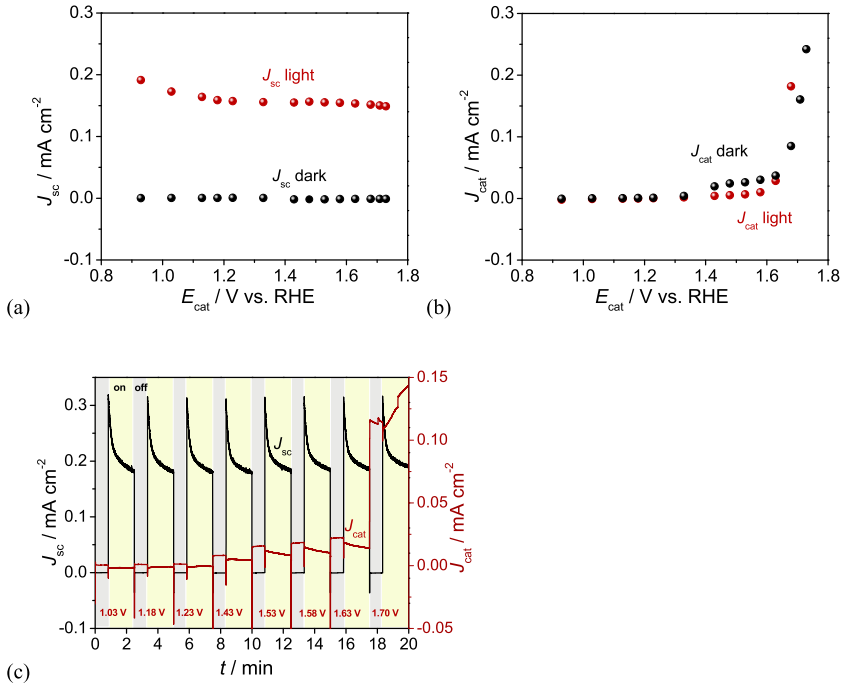

Figure 3. *In situ* measurement of the electrocatalyst and semiconductor current density. (a) J_{sc} was measured under illumination and in the dark from WE1. (b) J_{cat} was measured under illumination and in the dark from WE2. (c) *In situ* measurement of J_{sc} and J_{cat} under chopped illumination. All measurements were done by applying different potentials to the electrocatalyst, while the semiconductor potential was held at 1.23 V vs RHE.

is similar to that obtained from the electrode in the absence of the gold layer since backside illumination is utilized (*i.e.*, photons pass through the FTO side of the electrode first) (Figure S8). This similarity between $J-E$ curves confirms that the gold film does not have any measurable effect on the water oxidation activity. The $J-E$ response of $CuWO_4$ (black line in Figure 2a) shows a net positive current at $E_{sc} > 0.9$ V vs RHE. This can be ascribed to driving water oxidation on the $CuWO_4$ surface as well as on the electrocatalyst layer. However, for the latter to occur, the electrocatalyst layer should possess a sufficiently positive potential from the transfer of photogenerated holes.

The observation of a capacitive return wave measured from WE1 at 0.85 V vs RHE suggests that at least some of the photocurrent from $CuWO_4$ goes toward oxidizing the Ni75 electrocatalyst. To be more quantitative, the potential of the electrocatalyst was measured while controlling the semiconductor potential. The steady-state potential of Ni75 (E_{cat}) on the $CuWO_4$ surface was measured via WE2 while stepping the potential of $CuWO_4$ (E_{sc}) via WE1 under illumination and in the dark (Figure S9). In the dark, the electrocatalyst can only be oxidized through the leakage current of the $CuWO_4$ photoanode in anodic bias. Due to the lack of leakage current in the dark, E_{cat} remains essentially constant when E_{sc} is between 0.55 and 1.55 V vs RHE (Figure S10). Figure 2b shows the electrocatalyst steady-state potential under illumination at each applied E_{sc}. There is a sharp transition of E_{cat} from 0.6 to 1.3 V vs RHE, which happens at $E_{sc} \sim 0.7$ V vs RHE. The transition of E_{cat} is attributed to the transfer of photogenerated holes to the electrocatalyst, which oxidizes it and shifts its potential positive in accord with the Nernst equation. Interestingly, however, the E_{cat} transition stops at a potential of 1.3 V vs RHE, which is not as positive as the current onset potential of the electrocatalyst, ~1.6 V vs RHE. These results suggest that while some of the photogenerated holes transfer to the electrocatalyst, the potential of the electrocatalyst somehow becomes pinned at a potential insufficient to drive water oxidation. This further implies that water oxidation must occur from the $CuWO_4$ surface.

To verify whether water oxidation occurs at the surface of $CuWO_4$ or the electrocatalyst, the *in situ* J_{sc} and J_{cat} were measured under both illumination and in the dark while holding E_{sc} at 1.23 V (vs RHE) and controlling the E_{cat} by WE2 (Figure S11). Figure 3a shows the steady-state J_{sc} vs E_{cat} under illumination and in the dark. There is nearly zero dark current at the constant applied potential of 1.23 V vs RHE. Under illumination, however, the steady-state J_{sc} is ~0.15 mA cm^{-2}, which is anodic photocurrent generated by $CuWO_4$. Figure 3b shows J_{cat} at different potentials applied to the electrocatalyst under illumination and in the dark. The J_{cat} in the dark remains negligible up to $E_{cat} = 1.6$ V vs RHE, which is the current onset potential of the electrocatalyst, then the current density continues to increase with increasing applied potential. Irradiation of the device shows similar behavior with a small decrease in current density compared to that in the dark. Since the potential of the electrocatalyst was held at a series of constant potentials, if there is a transfer of photogenerated holes from semiconductor to the electrocatalyst, there will be a reduction of these holes to maintain the fixed E_{cat} that would result in a negative J_{cat} under illumination. The small difference between J_{cat} under illumination and in the dark suggests that net hole transfer to the electrocatalyst is not efficient.

The *in situ* current density of the electrocatalyst and semiconductor was also measured under chopped illumination. Figure 3c shows the steady-state J_{sc} and J_{cat} at different potentials applied to the electrocatalyst. Once the light is turned on, an anodic spike is observed that slowly reaches a steady state. This is attributed to the charging of the electrocatalyst. Once the light is turned off, the dark current

https://dx.doi.org/10.1021/acsami.0c14705
ACS Appl. Mater. Interfaces 2020, 12, 50592−50599

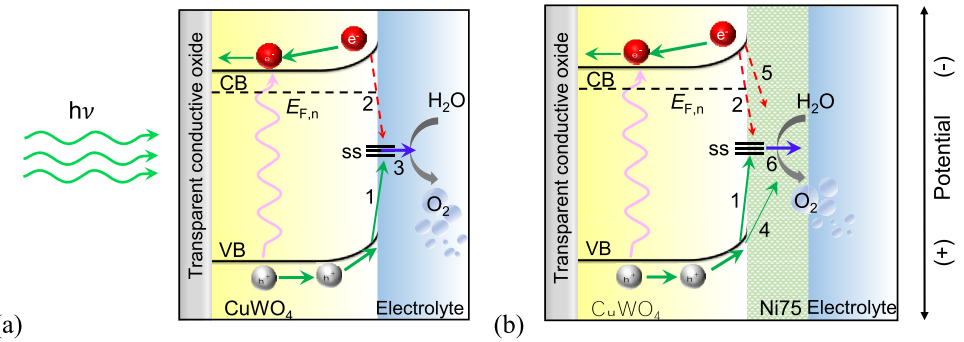

Figure 4. Simplified illustration of charge-transfer pathways in (a) bare and (b) Ni75-coated $CuWO_4$ under illumination. Green arrows represent the favorable processes (hole transfer to surface states (ss) (1) and to the electrocatalyst (4)), the dashed red arrows represent the unfavorable processes (recombination of electrons with holes in ss (2) and with holes accumulated in the electrocatalyst (5)), and the blue arrow indicates hole collection at the interface for water oxidation from ss (3) and from the electrocatalyst (6). For simplicity, the $E_{F,p}$ under illumination is not shown.

quickly drops to approximately zero. We found a negligible difference between J_{cat} under illumination to that in the dark. The difference between the J_{sc} under illumination and in the dark (ΔJ_{sc}) indicates the photoinduced hole current density at the surface of $CuWO_4$. By contrast, the quantity of the photogenerated holes transferred from the semiconductor to the electrocatalyst can be deduced from the difference between the J_{cat} under illumination and in the dark (ΔJ_{cat}). The ratio of $\Delta J_{cat}/\Delta J_{sc}$ then can be used to calculate the hole transfer efficiency from the semiconductor to the electrocatalyst layer, which based on the data in Figure 3 is a very small value (~7%). These results suggest that the integration of the electrocatalyst with $CuWO_4$ is not effective in driving water oxidation, and therefore water oxidation must occur almost exclusively at the semiconductor surface. This is consistent with the nominally identical $J-E$ curves for the bare and catalyst modified electrodes displayed in Figure 1c.

Figure 4 summarizes the charge-transfer processes that take place at the $CuWO_4$/electrolyte and $CuWO_4$/electrocatalyst interfaces. For the bare $CuWO_4$, photogenerated holes are transferred from the valance band to oxidize surface states (ss) (1). These oxidized surface states mediate water oxidation and may be intermediates in the water oxidation reaction analogous to hematite (3).[22,52] Water oxidation from these surface states is in kinetic competition with surface state recombination (2), which results in suboptimal current onset potential. With the addition of an electrocatalyst, direct hole transfer from the semiconductor to the electrocatalyst (4) competes with the surface hole trapping, and water oxidation can thus, in parallel, occur from the catalyst (6).[27,29] Storage of holes in the electrocatalyst introduces an additional recombination pathway for conduction band electrons (5).

Our surprising finding that water oxidation occurs primarily from the $CuWO_4$ surface rather than the Ni75 catalyst, therefore, implies that the rates of surface state hole trapping and water oxidation from these states is faster than hole transfer and water oxidation from the catalyst. It has been suggested that water oxidation from $CuWO_4$ is slow,[21] based on a Tafel analysis, whereas Ni75 is among the best (fastest) known water oxidation catalyst.[32] The photocurrent as a function of applied potential is not expected to follow the Tafel behavior of a conductive electrocatalyst but a convolution of the drift-diffusion limited flux of holes to the surface and potential-dependent surface state recombination.[53] Thus, we believe the actual rate of water oxidation on $CuWO_4$ is an open question and may actually be relatively fast. This suggestion is consistent with our finding of quantitative water oxidation efficiency once modest potentials have been applied to mitigate surface state recombination.[12] Thus, we hypothesize that the forward rate of water oxidation on $CuWO_4$ is not "slow," but the competing surface state recombination is fast. A more detailed analysis of these kinetic processes to unravel the surprising steady-state behavior found here is the subject of further investigation in our laboratory.

CONCLUSIONS

Systematic investigation of the charge-carrier dynamics at the interface of PPO-modified $CuWO_4$ photoanodes with the Ni75 electrocatalyst using the advanced DWE technique was utilized to shed light on the unusual response of the $CuWO_4$/electrocatalyst system for PEC water oxidation. Despite the incorporation of an electrocatalyst layer, the overall performance of the electrode does not improve relative to the bare electrode. *In situ* measurements of the electrocatalyst (Ni75) potential corroborate the transfer of photogenerated holes from the $CuWO_4$ valance band to the electrocatalyst. However, this transfer does not lead to a sufficiently positive potential of the electrocatalyst to drive the water oxidation. Instead, the reaction predominantly proceeds on the surface of $CuWO_4$, as revealed by *in situ* current density measurements. It is crucial to obtain a better understanding of the kinetics of the various electron and hole transfer reactions, which will require additional investigations with a larger suite of time-resolved methods that our lab is currently pursuing. The results of the steady-state measurements presented here, however, are important as they offer the first direct evidence that water oxidation on a semiconductor surface can outcompete water oxidation via a highly active cocatalyst. This result differs from all previously reported DWE measurements of PEC water oxidation systems.[54]

ASSOCIATED CONTENT

Supporting Information

The Supporting Information is available free of charge at https://pubs.acs.org/doi/10.1021/acsami.0c14705.

Structure of DWE, SEM images, and AFM analysis of bare and Ni75-coated $CuWO_4$, Raman spectra of bare FTO, and Ni75-coated $CuWO_4$ before and after UV irradiation, $J-E$ responses of $CuWO_4$ for water and Na_2SO_3 oxidation and that after PPO electrodeposition,

https://dx.doi.org/10.1021/acsami.0c14705
ACS Appl. Mater. Interfaces 2020, 12, 50592−50599

and *in situ* measurement of the electrocatalyst potential and current density (PDF)

AUTHOR INFORMATION

Corresponding Author

Thomas W. Hamann − *Department of Chemistry, Michigan State University, East Lansing, Michigan 48824-1322, United States;* orcid.org/0000-0001-6917-7494; Email: hamann@chemistry.msu.edu

Authors

Parisa Shadabipour − *Department of Chemistry, Michigan State University, East Lansing, Michigan 48824-1322, United States;* orcid.org/0000-0001-7490-3024

Austin L. Raithel − *Department of Chemistry, Michigan State University, East Lansing, Michigan 48824-1322, United States*

Complete contact information is available at: https://pubs.acs.org/10.1021/acsami.0c14705

Author Contributions

P.S. and T.W.H. designed the project. P.S. performed the experiments, characterizations, and analyzed the data. A.L.R. assisted with precursor synthesis. P.S. and T.W.H. discussed the results. P.S. and T.W.H. wrote the paper. T.W.H. supervised the project.

Notes

The authors declare no competing financial interest.

ACKNOWLEDGMENTS

T.W.H. gratefully acknowledges the financial support by NSF Award CHE-1664823.

REFERENCES

(1) Wang, G.; Wang, H.; Ling, Y.; Tang, Y.; Yang, X.; Fitzmorris, R. C.; Wang, C.; Zhang, J. Z.; Li, Y. Hydrogen-Treated TiO_2 Nanowire Arrays for Photoelectrochemical Water Splitting. *Nano Lett.* **2011**, *11*, 3026−3033.

(2) Chen, X.; Liu, L.; Yu, P. Y.; Mao, S. S. Increasing Solar Absorption for Photocatalysis with Black Hydrogenated Titanium Dioxide Nanocrystals. *Science* **2011**, *331*, 746−751.

(3) Hardee, K. L.; Bard, A. J. Semiconductor Electrodes. *J. Electrochem. Soc.* **1976**, *123*, 1024−1026.

(4) Kennedy, J. H.; Frese, K. W. Photooxidation of Water at Alfa-Fe_2O_3 Electrodes. *J. Electrochem. Soc.* **1978**, *125*, 709−714.

(5) Sivula, K.; Le Formal, F.; Grätzel, M. Solar Water Splitting: Progress Using Hematite (α-Fe_2O_3) Photoelectrodes. *ChemSusChem* **2011**, *4*, 432−449.

(6) Hodes, G.; Cahen, D.; Manassen, J. Tungsten Trioxide as a Photoanode for a Photoelectrochemical Cell (PEC). *Nature* **1976**, *260*, 312−313.

(7) Tamirat, A. G.; Rick, J.; Dubale, A. A.; Su, W.-N.; Hwang, B.-J. Using Hematite for Photoelectrochemical Water Splitting: A Review of Current Progress and Challenges. *Nanoscale Horiz.* **2016**, *1*, 243−267.

(8) Jeon, T. H.; Monllor-Satoca, D.; Moon, G.-H.; Kim, W.; Kim, H.-I.; Bahnemann, D. W.; Park, H.; Choi, W. Ag(I) Ions Working as a Hole-Transfer Mediator in Photoelectrocatalytic Water Oxidation on WO_3 Film. *Nat. Commun.* **2020**, *11*, No. 967.

(9) Lee, D. K.; Lee, D. K.; Lumley, M. A.; Choi, K.; Lee, D. K. Progress on Ternary Oxide-Based Photoanodes for Use in Photoelectrochemical Cells for Solar Water Splitting. *Chem. Soc. Rev.* **2018**, *48*, 2126−2157.

(10) Rajeshwar, K.; Hossain, M. K.; Macaluso, R. T.; Janáky, C.; Varga, A.; Kulesza, P. J. Review-Copper Oxide-Based Ternary and Quaternary Oxides: Where Solid-State Chemistry Meets Photoelectrochemistry. *J. Electrochem. Soc.* **2018**, *165*, H3192−H3206.

(11) Gao, Y.; Zandi, O.; Hamann, T. W. Atomic Layer Stack Deposition-Annealing Synthesis of $CuWO_4$. *J. Mater. Chem. A* **2016**, *4*, 2826−2830.

(12) Gao, Y.; Hamann, T. W. Quantitative Hole Collection for Photoelectrochemical Water Oxidation with $CuWO_4$. *Chem. Commun.* **2017**, *53*, 1285−1288.

(13) Yourey, J. E.; Bartlett, B. M. Electrochemical Deposition and Photoelectrochemistry of $CuWO_4$, a Promising Photoanode for Water Oxidation. *J. Mater. Chem.* **2011**, *21*, 7651−7660.

(14) Hill, J. C.; Choi, K.-S. Synthesis and Characterization of High Surface Area $CuWO_4$ and Bi_2WO_6 Electrodes for Use as Photoanodes for Solar Water Oxidation. *J. Mater. Chem. A* **2013**, *1*, 5006.

(15) Tian, C. M.; Jiang, M.; Tang, D.; Qiao, L.; Xiao, H. Y.; Oropeza, F. E.; Hofmann, J. P.; Hensen, E. J. M.; Tadich, A.; Li, W.; Qi, D. C.; Zhang, K. H. L. Elucidating the Electronic Structure of $CuWO_4$ Thin Films for Enhanced Photoelectrochemical Water Splitting. *J. Mater. Chem. A* **2019**, *7*, 11895−11907.

(16) Zhang, H.; Yilmaz, P.; Ansari, J. O.; Khan, F. F.; Binions, R.; Krause, S.; Dunn, S. Incorporation of Ag Nanowires in $CuWO_4$ for Improved Visible Light-Induced Photoanode Performance. *J. Mater. Chem. A* **2015**, *3*, 9638−9644.

(17) Pyper, K. J.; Yourey, J. E.; Bartlett, B. M. Reactivity of $CuWO_4$ in Photoelectrochemical Water Oxidation Is Dictated by a Midgap Electronic State. *J. Phys. Chem. C* **2013**, *117*, 24726−24732.

(18) Gaillard, N.; Chang, Y.; Deangelis, A.; Higgins, S.; Braun, A. A Nanocomposite Photoelectrode Made of 2.2 eV Band Gap Copper Tungstate ($CuWO_4$) and Multi-Wall Carbon Nanotubes for Solar-Assisted Water Splitting. *Int. J. Hydrogen Energy* **2013**, *38*, 3166−3176.

(19) Ye, W.; Chen, F.; Zhao, F.; Han, N.; Li, Y. $CuWO_4$ Nanoflake Array-Based Single-Junction and Heterojunction Photoanodes for Photoelectrochemical Water Oxidation. *ACS Appl. Mater. Interfaces* **2016**, *8*, 9211−9217.

(20) Bohra, D.; Smith, W. A. Improved Charge Separation via Fe-Doping of Copper Tungstate Photoanodes. *Phys. Chem. Chem. Phys.* **2015**, *17*, 9857−9866.

(21) Lhermitte, C. R.; Bartlett, B. M. Advancing the Chemistry of $CuWO_4$ for Photoelectrochemical Water Oxidation. *Acc. Chem. Res.* **2016**, *49*, 1121−1129.

(22) Gao, Y.; Hamann, T. W. Elucidation of $CuWO_4$ Surface States During Photoelectrochemical Water Oxidation. *J. Phys. Chem. Lett.* **2017**, *8*, 2700−2704.

(23) Liu, R.; Zheng, Z.; Spurgeon, J.; Yang, X. Enhanced Photoelectrochemical Water-Splitting Performance of Semiconductors by Surface Passivation Layers. *Energy Environ. Sci.* **2014**, *7*, 2504−2517.

(24) Zachäus, C.; Abdi, F. F.; Peter, L. M.; Van De Krol, R. Photocurrent of $BiVO_4$ Is Limited by Surface Recombination, Not Surface Catalysis. *Chem. Sci.* **2017**, *8*, 3712−3719.

(25) Barroso, M.; Cowan, A. J.; Pendlebury, S. R.; Grätzel, M.; Klug, D. R.; Durrant, J. R. The Role of Cobalt Phosphate in Enhancing the Photocatalytic Activity of α-Fe_2O_3 toward Water Oxidation. *J. Am. Chem. Soc.* **2011**, *133*, 14868−14871.

(26) Barroso, M.; Mesa, C. A.; Pendlebury, S. R.; Cowan, A. J.; Hisatomi, T.; Sivula, K.; Gratzel, M.; Klug, D. R.; Durrant, J. R. Dynamics of Photogenerated Holes in Surface Modified α-Fe_2O_3 Photoanodes for Solar Water Splitting. *Proc. Natl. Acad. Sci. U.S.A.* **2012**, *109*, 15640−15645.

(27) Klahr, B.; Gimenez, S.; Fabregat-Santiago, F.; Bisquert, J.; Hamann, T. W. Photoelectrochemical and Impedance Spectroscopic Investigation of Water Oxidation with "Co−Pi"-Coated Hematite Electrodes. *J. Am. Chem. Soc.* **2012**, *134*, 16693−16700.

(28) Carroll, G. M.; Gamelin, D. R. Kinetic Analysis of Photoelectrochemical Water Oxidation by Mesostructured Co-Pi/α-Fe_2O_3 Photoanodes. *J. Mater. Chem. A* **2016**, *4*, 2986−2994.

(29) Qiu, J.; Hajibabaei, H.; Nellist, M. R.; Laskowski, F. A. L.; Hamann, T. W.; Boettcher, S. W. Direct in Situ Measurement of

Charge Transfer Processes During Photoelectrochemical Water Oxidation on Catalyzed Hematite. *ACS Cent. Sci.* **2017**, *3*, 1015−1025.
(30) Davi, M.; Mann, M.; Ma, Z.; Schrader, F.; Drichel, A.; Budnyk, S.; Rokicinska, A.; Kustrowski, P.; Dronskowski, R.; Slabon, A. An MnNCN-Derived Electrocatalyst for $CuWO_4$ Photoanodes. *Langmuir* **2018**, *34*, 3845−3852.
(31) Xiong, X.; Fan, L.; Chen, G.; Wang, Y.; Wu, C.; Chen, D.; Lin, Y.; Li, T.; Fu, S.; Ren, S. Boosting Water Oxidation Performance of $CuWO_4$ Photoanode by Surface Modification of Nickel Phosphate. *Electrochim. Acta* **2019**, *328*, No. 135125.
(32) Trotochaud, L.; Young, S. L.; Ranney, J. K.; Boettcher, S. W. Nickel−Iron Oxyhydroxide Oxygen-Evolution Electrocatalysts: The Role of Intentional and Incidental Iron Incorporation. *J. Am. Chem. Soc.* **2014**, *136*, 6744−6753.
(33) Qiu, J.; Hajibabaei, H.; Nellist, M. R.; Laskowski, F. A. L.; Oener, S. Z.; Hamann, T. W.; Boettcher, S. W. Catalyst Deposition on Photoanodes: The Roles of Intrinsic Catalytic Activity, Catalyst Electrical Conductivity, and Semiconductor Morphology. *ACS Energy Lett.* **2018**, *3*, 961−969.
(34) Smith, R. D. L.; Prevot, M. S.; Fagan, R. D.; Zhang, Z.; Sedach, P. A.; Siu, M. K. J.; Trudel, S.; Berlinguette, C. P. Photochemical Route for Accessing Amorphous Metal Oxide Materials for Water Oxidation Catalysis. *Science* **2013**, *340*, 60−63.
(35) Shadabipour, P.; Hamann, T. W. Interface Passivation to Overcome Shunting in Semiconductor−Catalyst Junctions. *Chem. Commun.* **2020**, *56*, 2570−2573.
(36) Liu, R.; Lin, Y.; Chou, L. Y.; Sheehan, S. W.; He, W.; Zhang, F.; Hou, H. J. M.; Wang, D. Water Splitting by Tungsten Oxide Prepared by Atomic Layer Deposition and Decorated with an Oxygen-Evolving Catalyst. *Angew. Chem., Int. Ed.* **2011**, *50*, 499−502.
(37) Forsberg, J. H.; Spaziano, V. T.; Balasubramanian, T. M.; Liu, G. K.; Kinsley, S. A.; Duckworth, C. A.; Poteruca, J. J.; Brown, P. S.; Miller, J. L. Use of Lanthanide(III) Ions as Catalysts for the Reactions of Amines with Nitriles. *J. Org. Chem.* **1987**, *52*, 1017−1021.
(38) Li, Z.; Bary, T. S.; Gordon, G. R. Synthesis and Characterization of Copper (I) Amidinates as Precursors for Atomic Layer Deposition (ALD) of Copper Metal. *Inorg. Chem.* **2005**, *44*, 1728−1735.
(39) Hajibabaei, H.; Schon, A. R.; Hamann, T. W. Interface Control of Photoelectrochemical Water Oxidation Performance with $Ni_{1-x}Fe_xO_y$ Modified Hematite Photoanodes. *Chem. Mater.* **2017**, *29*, 6674−6683.
(40) Gregg, B. A.; Pichot, F.; Ferrere, S.; Fields, C. L. Interfacial Recombination Processes in Dye-Sensitized Solar Cells and Methods to Passivate the Interfaces. *J. Phys. Chem. B* **2001**, *105*, 1422−1429.
(41) Young, K. M. H.; Hamann, T. W. Enhanced Photocatalytic Water Oxidation Efficiency with $Ni(OH)_2$ Catalysts Deposited on α-Fe_2O_3 via ALD. *Chem. Commun.* **2014**, *50*, 8727−8730.
(42) McDonald, K. J.; Choi, K. S. Photodeposition of Co-Based Oxygen Evolution Catalysts on α-Fe_2O_3 Photoanodes. *Chem. Mater.* **2011**, *23*, 1686−1693.
(43) Kim, T. W.; Choi, K.-S. Nanoporous $BiVO_4$ Photoanodes with Dual-Layer Oxygen Evolution Catalysts for Solar Water Splitting. *Science* **2014**, *343*, 990−995.
(44) Nellist, M. R.; Qiu, J.; Laskowski, F. A. L.; Toma, F. M.; Boettcher, S. W. Potential-Sensing Electrochemical AFM Shows CoPi as a Hole Collector and Oxygen Evolution Catalyst on $BiVO_4$ Water-Splitting Photoanodes. *ACS Energy Lett.* **2018**, *3*, 2286−2291.
(45) Badia-Bou, L.; Mas-Marza, E.; Rodenas, P.; Barea, E. M.; Fabregat-Santiago, F.; Gimenez, S.; Peris, E.; Bisquert, J. Water Oxidation at Hematite Photoelectrodes with an Iridium-Based Catalyst. *J. Phys. Chem. C* **2013**, *117*, 3826−3833.
(46) Zhong, D. K.; Gamelin, D. R. Photoelectrochemical Water Oxidation by Cobalt Catalyst ("Co−Pi")/α-Fe_2O_3 Composite Photoanodes: Oxygen Evolution and Resolution of a Kinetic Bottleneck. *J. Am. Chem. Soc.* **2010**, *132*, 4202−4207.
(47) Seabold, J. A.; Choi, K. S. Effect of a Cobalt-Based Oxygen Evolution Catalyst on the Stability and the Selectivity of Photo-Oxidation Reactions of a WO_3 Photoanode. *Chem. Mater.* **2011**, *23*, 1105−1112.
(48) Abdi, F. F.; Firet, N.; van de Krol, R. Efficient $BiVO_4$ Thin Film Photoanodes Modified with Cobalt Phosphate Catalyst and W-Doping. *ChemCatChem* **2013**, *5*, 490−496.
(49) Riha, S. C.; Klahr, B. M.; Tyo, E. C.; Seifert, S.; Vajda, S.; Pellin, M. J.; Hamann, T. W.; Martinson, A. B. F. Atomic Layer Deposition of a Submonolayer Catalyst for the Enhanced Photoelectrochemical Performance of Water Oxidation with Hematite. *ACS Nano* **2013**, *7*, 2396−2405.
(50) Chang, X.; Wang, T.; Zhang, P.; Zhang, J.; Li, A.; Gong, J. Enhanced Surface Reaction Kinetics and Charge Separation of p−n Heterojunction Co_3O_4/$BiVO_4$ Photoanodes. *J. Am. Chem. Soc.* **2015**, *137*, 8356−8359.
(51) Lin, F.; Boettcher, S. W. Adaptive Semiconductor/Electrocatalyst Junctions in Water-Splitting Photoanodes. *Nat. Mater.* **2014**, *13*, 81−86.
(52) Zandi, O.; Hamann, T. W. Determination of Photoelectrochemical Water Oxidation Intermediates on Haematite Electrode Surfaces Using Operando Infrared Spectroscopy. *Nat. Chem.* **2016**, *8*, 778−783.
(53) Zandi, O.; Hamann, T. W. The Potential versus Current State of Water Splitting with Hematite. *Phys. Chem. Chem. Phys.* **2015**, *17*, 22485−22503.
(54) Laskowski, F. A. L.; Nellist, M. R.; Qiu, J.; Boettcher, S. W. Metal Oxide/(Oxy)Hydroxide Overlayers as Hole Collectors and Oxygen-Evolution Catalysts on Water-Splitting Photoanodes. *J. Am. Chem. Soc.* **2019**, *141*, 1394−1405.

https://dx.doi.org/10.1021/acsami.0c14705
ACS Appl. Mater. Interfaces 2020, 12, 50592−50599